Title

Indispensable Nafion Ionomer for High-Efficiency and Stable Oxygen Evolution Reaction in Alkaline Media.

Journal

ACS Applied Materials & Interfaces, 15(48)

Authors

Kakati, Nitul

Anderson, Lawrence

Li, Guangfu

et al.

Publication Date

2023-12-06

DOI

10.1021/acsami.3c08377

Peer reviewed

ACS APPLIED MATERIALS & INTERFACES

www.acsami.org

Research Article

Indispensable Nafion Ionomer for High-Efficiency and Stable Oxygen Evolution Reaction in Alkaline Media

Nitul Kakati, Lawrence Anderson, Guangfu Li,* Desiree Mae Sua-an, Ayon Karmakar, Joey D. Ocon, and Po-Ya Abel Chuang*

Cite This: *ACS Appl. Mater. Interfaces* 2023, 15, 55559−55569

Read Online

ACCESS | Metrics & More | Article Recommendations | Supporting Information

ABSTRACT: Addressing the challenge of sluggish kinetics and limited stability in alkaline oxygen evolution reactions, recent exploration of novel electrochemical catalysts offers improved prospects. To expedite the assessment of these catalysts, a half-cell rotating disk electrode is often favored for its simplicity. However, the actual catalyst performance strongly depends on the fabricated catalyst layers, which encounter mass transport overpotentials. We systematically investigate the role and sequence of electrode drop-casting methods onto a glassy carbon electrode regarding the efficiency of the oxygen evolution reaction. The catalyst layer without Nafion experiences nearly 50% activity loss post stability test, while those with Nafion exhibit less than 5% activity loss. Additionally, the sequence of application of the catalyst and Nafion also shows a significant effect on catalyst stability. The catalyst activity increases by roughly 20% after the stability test when the catalyst layer is coated first with an ionomer layer, followed by drop-casting the catalysts. Based on the half-cell results, the Nafion ionomer not only acts as a binder in the catalyst layer but also enhances the interfacial interaction between the catalyst and electrolyte, promoting performance and stability. This study provides new insights into the efficient and accurate evaluation of electrocatalyst performance and stability as well as the role of Nafion ionomer in the catalyst layer.

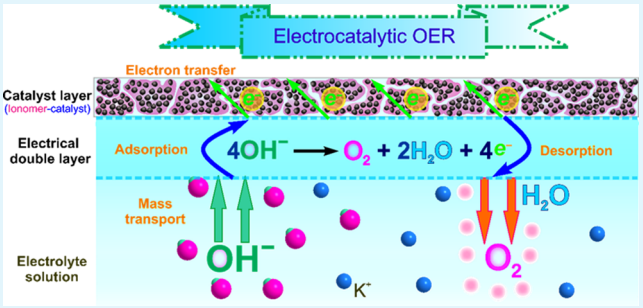

KEYWORDS: *oxygen evolution reaction, TF-RDE/RRDE, catalyst layer structure, Nafion ionomer, drop-casting*

1. INTRODUCTION

The rising energy demand and depleting fossil fuel supplies have shifted global attention to renewable and sustainable energy technologies, including hydrogen energy as a clean alternative fuel.[1] However, the technologies for producing hydrogen from new and renewable energy sources are not yet matured, and the cost of production remains very high and uncompetitive compared with that generated from fossil fuels. Currently, around 95% of generated hydrogen originates from carbonaceous raw materials, mostly of fossil origin, with just 4% generated by water electrolysis.[2] In comparison to acidic electrolysis, liquid alkaline electrolysis is a more well-developed technology. Alkaline electrolysis is less costly as it employs non-noble-metal electrocatalysts such as Ni, Co, Fe, Mn, and Mo.[3−8] Additionally, compared to that in the alkaline medium, significant corrosion can be observed in an acidic medium.

In water electrolysis reactions, the oxygen evolution reaction (OER) is much more sluggish compared with the hydrogen evolution reaction (HER) due to slow kinetics. Therefore, considerable research effort has been made to enhance the activity of the OER by using different catalyst materials. The need for noble-metal catalysts, such as IrO_x and RuO_2, as well as their poor kinetic performance, are primary challenges in proton exchange membrane water electrolysis.[9,10] When water electrolysis is performed in alkaline media, the use of noble-metal catalysts can be reduced or eliminated entirely. With the rising interest in alkaline anion exchange membrane water electrolysis, there is a greater need for more sophisticated and less costly OER catalysts.[11−14] In the past few decades, research and development on the activity and long-term stability researches have resulted in substantial improvements in OER catalysts.[15−18] However, correctly assessing actual catalyst performance in alkaline media remains a challenge.[19−22] The results from a three-electrode system based on a thin film rotating disk electrode (TF-RDE) and thin film rotating ring disk electrode (TF-RRDE) are widely used to estimate catalyst performance in a full electrochemical cell.[23−29] However, ambiguities arise in the majority of the TF-RDE/RRDE results due to the numerous process steps involved in ink production

Received: June 10, 2023
Revised: October 25, 2023
Accepted: November 6, 2023
Published: November 21, 2023

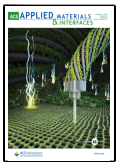

and deposition on the electrode surface, operating conditions, and multiple measurement methodologies. In their study, Riasse et al. compared various methods of catalyst evaluation, including RDE, gas diffusion electrode, and differential cell.[30] Each method exhibited its own set of advantages and drawbacks. In specific, the RDE study demonstrated high mass transport limitations but offered a clean experimental environment and ease of operation and notably required only a small quantity of catalyst for the investigation.

Nafion ionomer is commonly employed in TF-RDE/RRDE studies as a dispersion for catalyst particles in catalyst ink as well as a binder to prevent the catalyst layer (CL) from peeling off the electrode surface.[31−33] The CL coated on the electrode surface is known to have a significant impact on the electrochemical performance.[34] The key parameters that influence electrochemical characteristics are typically linked to the morphology of the catalyst ink, the coating technique, and the drying processes.[35,36] In diverse electrochemical processes, such as proton exchange membrane fuel cells (PEMFCs) and anion exchange membrane fuel cells (AEMFCs), several authors have described the relevance of the ionomer in the catalyst ink with an optimal ionomer-to-catalyst ratio.[37−40] Due to the absence of contrast between Nafion and the catalyst particles, imaging the CL under a state-of-the-art electron microscope to obtain information on Nafion morphology and transport behavior is very challenging.[41] As a result, electrochemical techniques have attracted more attention as an effective method to investigate and understand the CL's interfacial mechanism and electrochemical behavior, revealing the function of the ionomer in the CL.

In a recent research, we employed in situ and ex situ methods to analyze the critical function of Nafion and provide new insights into how the presence of the Nafion ionomer in the CL affects the electrical double layer (EDL) structure.[24] The importance of the ionomer in the alkaline OER is a crucial but relatively understudied aspect. The ionomer plays a significant role in determining the properties of the ink and the physical and electrochemical behaviors of the catalyst layers (CLs), particularly at the reaction EDL interface. In our recent study, the CL containing Nafion exhibited the highest OER activity in the alkaline medium compared to those prepared using the anion exchange ionomer (AEI) As-4 (Tokuyama Corp.) and the nonionic PTFE binder (Fuel Cell Store).[24] Lu et al. conducted research on an imidazolium-functionalized poly(ether sulfone) as an AEI for use in fuel cells. They compared its electrochemical characteristics with those of AS-4 and Nafion ionomers.[42] In their study, the researchers also found that the Pt/C catalyst using the Nafion ionomer showed the highest mass activity. Even though the goal for alkaline OER is to eliminate the use of precious metal and perfluoroalkyl substances (PFAs), Nafion is still the most commonly used in preparing catalyst ink for evaluating electrocatalyst activities. Therefore, in the present study, we have expanded our investigation to study the influence of Nafion and CL coating processes on the activity and stability of the OER in an alkaline medium. The objective of this investigation is to develop a fundamental understanding of how the Nafion ionomer in catalyst inks affects the CL and impacts the OER mechanism of the IrO_x catalyst.

2. EXPERIMENTAL SECTION

2.1. Chemical Reagents. Potassium hydroxide (KOH, ≥90 wt %), anhydrous ethanol (≥95 wt %), and 1 wt % Nafion solution were purchased from Sigma-Aldrich. Iridium oxide (IrO_x, 99.99%) was obtained from Alfa Aesar. Solutions were prepared by using ultrapure deionized water (18 MΩ cm resistivity) supplied by an in-house water purification system from Thermo Scientific Barnstead Nanopure.

2.2. Structural Characterization. The Zeiss Gemini field emission scanning electron microscope (FESEM) 500 operating at 5 kV was used to capture the SEM images. The IrOx-based catalyst ink was drop-cast onto a glassy carbon electrode (GCE) for all SEM samples.

2.3. Electrochemical Tests. A bipotentiostat (CHI 750E) was used to conduct the electrochemical tests at room temperature and ambient pressure. A Hg/HgO electrode (filled with 1 M KOH), a platinum wire (7 mm OD × 65 mm), and an RDE/RRDE were used as the reference electrode (RE), counter electrode (CE), and working electrode (WE), respectively, in a standard three-electrode system. The RDE (E3, Pine Instrument Co.) had a GCE with an outer diameter (OD) of 5 mm, and the RRDE (E7R9, Pine Instrument Co.) had a submillimeter gap between its GCE disk (5.61 mm OD) and platinum ring (7.92 mm OD, 6.25 mm ID). The calibrated potential of the applied Hg/HgO reference electrode vs the reversible hydrogen electrode (RHE) in 1 M KOH at room temperature was found to be 0.898 V. A 300 mL PTFE cell filled with N_2-saturated 6 M KOH was used to immerse the three-electrode system. To examine the influence of catalyst configuration on the electrochemical behavior of the OER, the catalyst ink was deposited over the GCE in four distinct ways. In the first mode, the catalyst ink was prepared by dispersing 5 mg of IrO_x in 4 mL of ethanol through sonication and drop-cast without the use of Nafion electrolyte (No-I); in the second mode, it was prepared by combining catalyst powder (IrO_x), ethanol, and 1% Nafion ionomer (Mix-I); and in the third mode, a drop of 1% Nafion ionomer was cast first, and then after drying the ionomer under an IR lamp, catalyst ink prepared without mixing ionomer was drop-cast over the Nafion ionomer layer. In the fourth mode, the processes in the third mode were reversed; i.e., the CL was deposited first, and the ionomer layer was deposited over the CL.

The standard catalyst loading was maintained at 0.08 mg cm^{-2} throughout the experiment. We also investigated the influence of catalyst loading on the electrochemical performance by using a higher loading of 0.24 mg cm^{-2}. In addition, to investigate the configurational influence of CLs on electrochemical characteristics, we synthesized CLs with three layers, such as ionomer-catalyst-ionomer (I−C−I) and catalyst-ionomer-catalyst (C−I−C), and compared their catalytic efficiency toward OER with their two-layer equivalent. In all CLs, the catalyst-to-ionomer ratio was kept constant. Cyclic Voltammetry tests were performed under static conditions (rotating speed = 0), and a standard electrode rotating speed of 1600 rpm was used while performing the linear scanning voltammetry (LSV) and electrochemical impedance spectroscopy (EIS) to facilitate mass transport and O_2 removal from the reaction interface. For accelerated stability evaluation, pulsed chronoamperometry was used with a pulse width of 30 s. The potentials were pulsed at 1.45 and 1.55 V vs RHE and completed 60 steps in 1800 s and the LSV and EIS were compared with those before the stability tests.

The effect of the ink coating technique on the EDL charging process and the efficiency of transporting the O_2 during the OER was demonstrated using TF-RRDE experiments. Standard voltammetry curves were obtained at a rotating speed of 1600 rpm while the disk potential was increasing with time and the ring potential was held at 0.4 V for oxygen reduction reaction. The geometric collection efficiency of the RRDE was measured to be 37.3% by detecting the redox couple $[Fe(CN)_6]^{3-}/[Fe(CN)_6]^{4-}$. To evaluate the ring collection efficiency for a gas-evolving reaction, hydrogen evolution has been chosen as a model reaction at the disk electrode with a commercial Pt/C catalyst in accordance with Chung et al.[43] The catalyst ink was prepared by dispersing 3 mg of commercial Pt/C (46.8%) powder in 2 mL of ethanol and 27 μL of Nafion solution (5 wt %) for 30 min under sonication. To prepare the working electrode, 40 μL of the resultant ink was drop-cast only on the glassy carbon (GC) disk of an RRDE electrode with the Pt-ring. After being dried under the IR lamp, LSV curves were recorded by the RRDE in N_2-saturated 0.1 M KOH by sweeping the potential from 0.1 to −0.23 V vs RHE at the GC-disk for

https://doi.org/10.1021/acsami.3c08377
ACS Appl. Mater. Interfaces 2023, 15, 55559−55569

HER and the ring potential was held at 0.2 V vs RHE. The collection efficiency was calculated from the ratio of the absolute value of the current responses at the ring to disk and found to range between 40% (low current) and 18% (high current) as shown in Figure S12. The collection efficiency of the realistic hydrogen evolution reaction stabilizes at around 18.1%, which is much less than the geometric collection efficiency obtained from the redox couple $[Fe(CN)_6]^{3-}/[Fe(CN)_6]^{4-}$ mainly due to bubble formation.

3. RESULTS AND DISCUSSION

Oxygen evolution reaction involves complicated multisteps of electrochemical reactions occurring near the catalyst surface. Figure 1 presents a schematic depiction of the reaction process

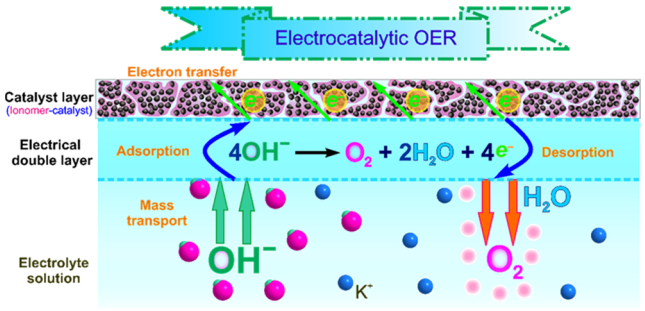

Figure 1. Schematic illustration of the interfacial OER with emphases on the mass transport behaviors in alkaline media.

at the EDL area, which constitutes the interface between the catalyst surface and the electrolyte. At the applied OER potential, the Coulombic attraction between OH^- ions and CL causes the adsorption of OH^- ions on the active CL. The OER electrocatalysts layer facilitates the faradaic conversion of OH^- ions into electrons, water, and oxygen. The rate of the OER depends on the number of available active electrocatalyst sites, as well as the OH^- ions, electrons, and O_2-transport resistances in the EDL.[44,45]

The different modes of catalyst and Nafion deposition on the surface of a GCE are illustrated schematically in Figure 2. Under mode 1, the CL does not include the ionomer, while in mode 2, the catalyst ink is formulated with the ionomer. Mode 3 involves the deposition of a Nafion ionomer layer on the GCE, followed by the deposition and drying of the catalyst ink over the ionomer layer. In mode 4, the process is reversed, with the catalyst ink being deposited and dried on the GCE, followed by the application of a second layer of the Nafion ionomer. The presence of Nafion ionomer with CL can act as a binder, preventing catalyst loss and increasing the reaction interface. Additionally, our previous studies have shown that the ζ-potential of catalyst inks increases with the amount of Nafion ionomer in the ink, resulting in enhanced electrostatic repulsion between the catalyst agglomerates and improved ink stability.[24,27]

SEM images of CLs on GCE without and with Nafion ionomer are presented in Figure 3a,3b, respectively. These images demonstrate the significant impact of the Nafion ionomer on the dispersion of the catalyst ink. Without the ionomer, the dispersion of the catalyst ink is negatively affected, leading to the formation of large particle aggregates, decreased active surface area, and reduced catalyst utilization. The CV curves reveal a distinctive "fingerprint" region in the potential range of 0.4−1.4 V for IrO_x,[46] as observed in Figure 3c. The current shown in Figure 3c encompasses both the EDL charging process and the pseudocapacitive current resulting from redox processes. To isolate the influence of pseudocapacitance, CV curves in Figure S1 were derived from Figure 3c within the potential range of 0.8−1.0 V. The rectangular-like shape of the CV curves in Figure S1 confirms the pure non-Faradaic capacitive behavior.[47] Figure 3d displays the experiment measurements of single-point anodic and cathodic currents at 0.9 V for various scan rates ranging from 2 to 150 mV s^{-1} and linearly fitted line over a scan rate range of 2−100 mV s^{-1}. The slopes of the linear fitting of the single-point currents at different scan rates provide information about the EDL capacitance and, subsequently, an estimate of the trend in the electrocatalytic

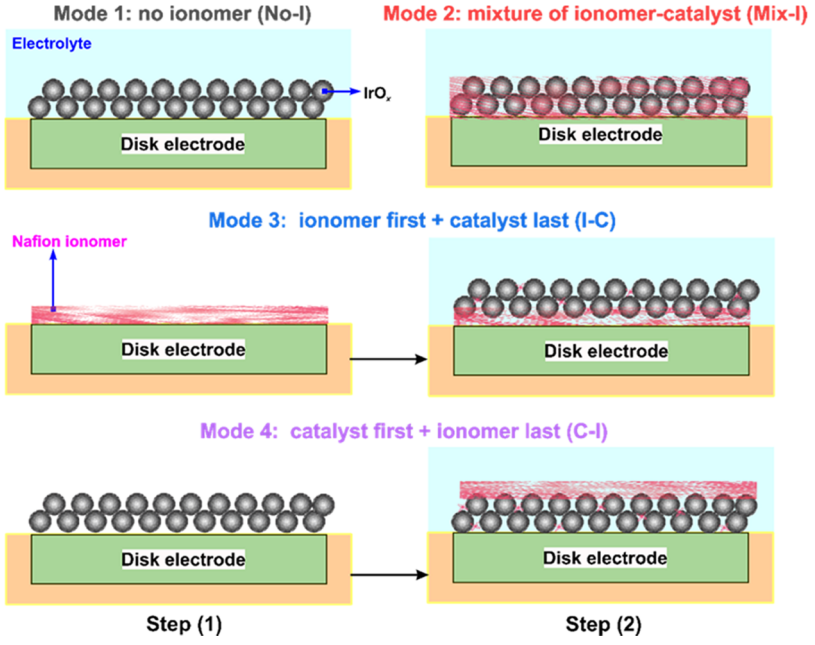

Figure 2. Illustration of the four Nafion ionomer deposition modes in the CLs for TF-RDE/RRDE evaluation.

https://doi.org/10.1021/acsami.3c08377
ACS Appl. Mater. Interfaces 2023, 15, 55559−55569

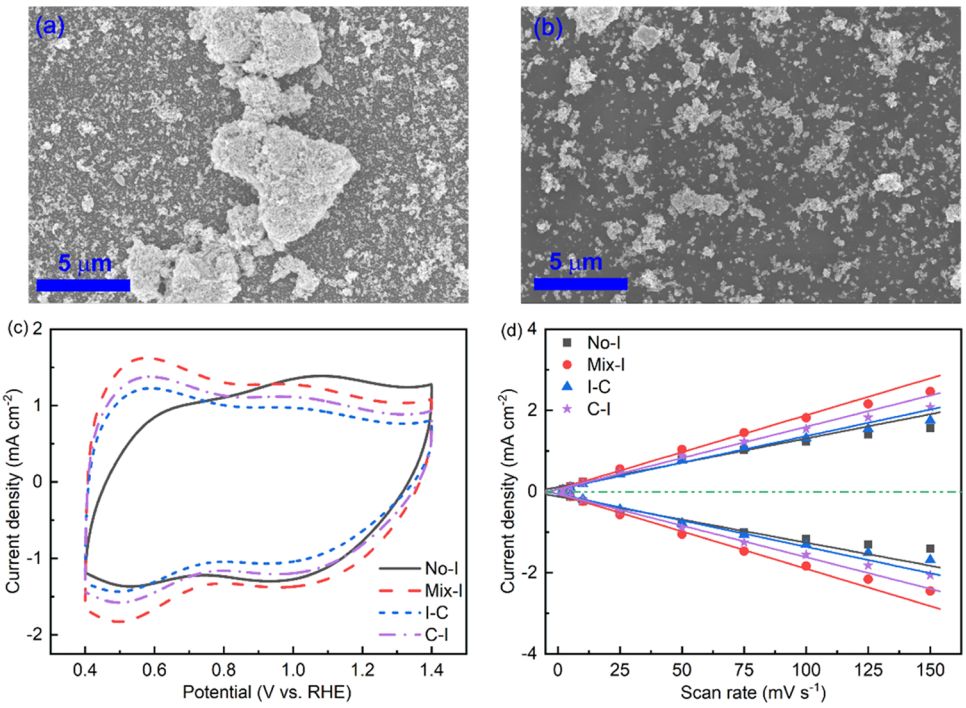

Figure 3. SEM images of the IrO_x CLs using inks (a) without ionomer and (b) with mixed ionomer. Electrochemical data of the (c) pseudocapacitive CV curves at 50 mV s^{-1} and (d) anodic (above zero) and cathodic (below zero) EDL capacitive current density at 0.9 V as a function of scan rate (symbols represent raw data and the lines are linearly fitted results in the scan rate range of 2−100 mV s^{-1}).

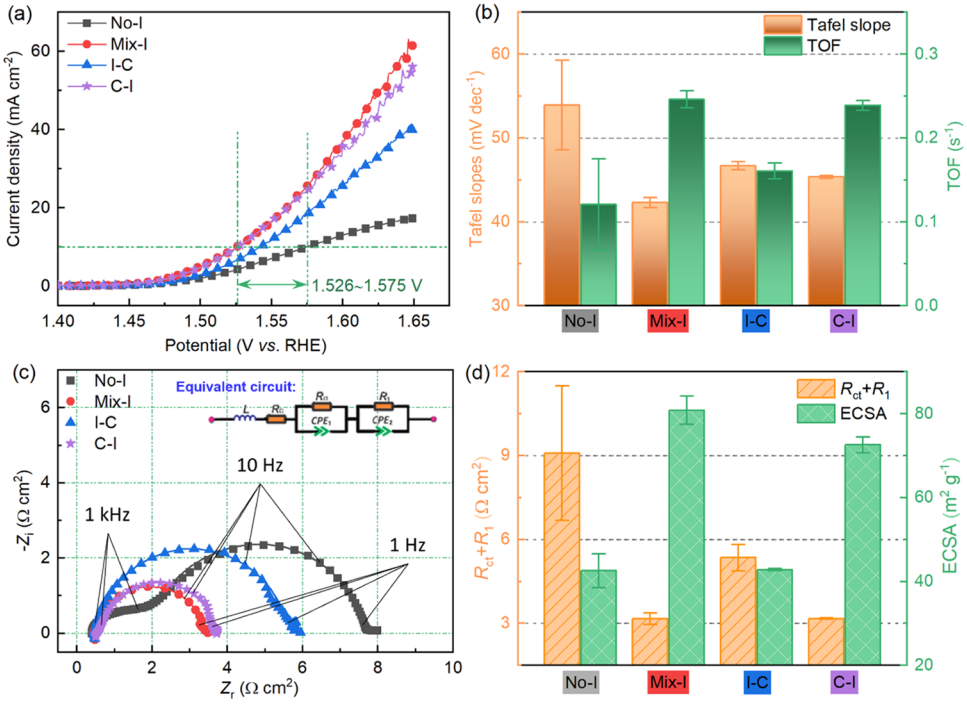

Figure 4. Electrocatalytic activity evaluation as a function of ionomer coating modes. (a) LSV curves at 2 mV s^{-1}, (b) Tafel slopes fitted between 0.3 and 3 mA cm^{-2} and TOF at *iR*-corrected voltage of 1.58 V, (c) EIS spectra at 1.55 V, the inset is the equivalent circuit for EIS simulation (symbols: raw data; lines: simulation results), and (d) the calculated total polarization resistance ($R_{ct} + R_1$) and ECSA. Error bars represent standard deviations from two independent measurements.

surface area (ECSA) of the CLs. From Figure 3d, the ECSA of the CLs decreases in the following order: Mix-I > C−I > I−C > No-I. In a previous study, we demonstrated that the ECSA calculated using the EIS approach is more accurate than the CV method.[25] Therefore, in this study, we analyzed the ECSA using the EIS approach and compared the trend to the CV method.

The electrocatalytic activity of the various CLs was evaluated by obtaining LSV curves at a scan rate of 2 mV s^{-1}. Figure 4a shows the LSV curves obtained from TF-RDE experiments at a

https://doi.org/10.1021/acsami.3c08377
ACS Appl. Mater. Interfaces 2023, 15, 55559−55569

rotating speed of 1600 rpm. CLs coated with Nafion ionomer had a significantly lower overpotential in the kinetic region (10 mA cm^{-2}) compared with CLs without Nafion (No-I). The overpotential for No-I increased by approximately 47 mV compared to Mix-I and C−I. Mix-I and C−I had overpotentials that were similar to, but lower than, No-I and I−C. It is important to note that the overpotential is influenced by both the kinetic and mass transport effects in the high-current-density region. No-I and I−C showed a larger increase in overpotential in the high-current-density region compared to Mix-I and C−I. Despite having identical overpotentials, C−I performed slightly worse in the high-current-density zone, possibly due to mass transport limitations imposed by the Nafion ionomer layer on top of the CL.[24] In Figure S2, the SEM image of the C−I mode shows the ionomer layer covering the catalyst particles.

To further evaluate the OER performance of the CLs, *IR*-free turnover frequency (TOF) and Tafel plots were analyzed based on the Tafel slopes (Figures 4b and S3). The OER is widely recognized as a four-electron transfer process, encompassing a series of stages and numerous intermediate species like MO, MOOH, or physically adsorbed peroxide species.[48] Over the course of many years, several potential pathways have been suggested for the mechanism. Among these, the Krasil'shchikov's path mechanism[25] holds prominence, which is outlined below with their corresponding Tafel slopes.

$$M + OH^- \leftrightarrow MOH + e^- \quad b = 120\,mV\,dec^{-1} \tag{1}$$

$$MOH + OH^- \leftrightarrow MO^- + H_2O \quad b = 60\,mV\,dec^{-1} \tag{2}$$

$$MO^- \rightarrow MO + e^- \quad b = 45\,mV\,dec^{-1} \tag{3}$$

$$2MO \rightarrow 2M + O_2 \quad b = 19\,mV\,dec^{-1} \tag{4}$$

The Tafel slopes in Figure 4b are obtained from the transport-free reaction kinetics data in the region of 0.3−3 mA cm^{-2} scanned at 2 mV s^{-1} to ensure minimal capacitive current (see also Figure S3b). The Tafel slope, which is close to 45 mV dec^{-1} for CLs containing Nafion, indicates the formation of surface-adsorbed *O intermediate.[25,26] However, No−I exhibited a substantially larger Tafel slope in the kinetic region. This phenomenon can be ascribed to the increase in bond strength of OH^- adsorption on catalysts containing Nafion, leading to a faster progression of the initial electron reaction depicted in eq 1, thereby enhancing electrocatalytic kinetics.[48] On the other hand, the change in Tafel slopes can also reflect the concentration of active sites and their contribution.[25] Therefore, it is likely that in this kinetic region, the thin Nafion layer covering the catalyst surface promotes the OER. In the high-current-density region (10−30 mA cm^{-2}), the Tafel slopes of the CLs were significantly higher than those in the low-current-density region. The elevation in the Tafel slope can be ascribed to four underlying mechanisms: (i) enhanced resistance to mass transport of OH^- ions, electrons, and/or O_2 molecules, (ii) alteration in the rate-determining step (RDS), (iii) adsorption of intermediates within the reaction, and (iv) modification of active sites and their involvement due to EDL reconstruction. The formation of O_2 bubbles obstructing the accessible reaction surface results in additional resistance to mass transport.[49,50] This hinders the adsorption of OH^- ions and the transport of electrons within the EDLs. To effectively mitigate the presence of O_2 bubbles and enhance mass transport, a frequently employed strategy is to raise the rotational speed of the WE. In our previous study,[25] we observed that elevating the rotational speed from 500 to 1600 rpm led to a marginal improvement in the OER performance. Mix-I had a TOF that was almost double that of No−I, suggesting that the presence of Nafion enhances both the interconnection among catalyst particles and the intrinsic activity toward OER.

The EDL during the OER is influenced by complex processes such as charge accumulation, transfer, and dissipation.[51] The interfacial behaviors in the EDL were evaluated by using Electrochemical Impedance Spectroscopy (EIS) as an in situ characterization tool. The EIS spectra were collected at an applied DC potential of 1.55 V. The modeled equivalent circuit and simulated Nyquist plots from EIS are presented in Figure 4c. Different CLs exhibited significant variations in impedance, indicating that the catalyst drop-casting modes play an important role in electron transport, reaction polarization resistance, and EDL capacitive behaviors. The values of various impedance fitting parameters based on the EIS equivalent circuit are provided in Table S1. In the inset of Figure 4c, the equivalent circuit $LR_\Omega(R_{ct}C_1)(R_1C_2)$ is used to fit and quantify the fitting parameters in the EIS spectra. In the equivalent circuit L, R_Ω, R_{ct}, C_1, R_1, and C_2 represent inductance, ohmic resistance, charge transfer resistance, EDL charging capacitance, intermediate diffusion/adsorption resistance, and capacitance, respectively.[25] In the equivalent circuit, two time-constant processes: charge transfer process and diffusion process in porous media are represented by $R_{ct}C_1$ and R_1C_2, respectively.[52,53] To simulate nonideal capacitances arising from heterogeneity, surface porosity, and EDL reconstruction, a constant phase element (CPE) is used, such as C_1 and C_2.[54,5554,55] The simulated results are consistent with the experimental data demonstrating the accurate representation of the OER process occurring in the EDL.

The ohmic resistance (R_Ω), total polarization resistance (R_{ct} + R_1), and electrochemical surface area (ECSA) were calculated by using the EIS simulated data (Table S1). The trends in total polarization resistance and ECSA as a function of CL casting modes are listed in Figure 4d. A detailed derivation of the ECSA from EIS data is reported in our previous study.[25] Higher ECSA is associated with lower total polarization resistance, indicating that the interaction of the Nafion ionomer with catalyst particles plays a crucial role in the OER performance. Although No-I and I−C have identical ECSAs, I−C exhibits a substantially lower total polarization resistance. The presence of the Nafion ionomer in I−C is believed to contribute to a reduction in charge transfer resistance, intermediate diffusion, and adsorption during OER.

The stability of the catalyst was assessed in 6 M KOH for 30 min using CA and a double-potential holding steps technique. Figure S4 depicts the detailed potential profile, which includes a high potential (1.55 V) step followed by a low potential step (1.45 V). El Sayed et al.[49] conducted an investigation into catalyst degradation caused by micro bubble formation on the catalyst layer. They observed that the catalyst layer remained stable under low current density (5.5 mA cm^{-2}) for several hours, while at high-current-density (27.5 mA cm^{-2}) operation, the stability reduced to about 30 min. As found in their study, controlling the electrode at the open circuit potential (OCP) and subsequently purging the RDE setup with argon (Ar) allows the dissolution and diffusion processes to effectively eliminate the O_2 bubbles. In our study, we assume that during the 30 s hold period at a low potential, the O_2 generated during the OER at the high potential can be efficiently eliminated. The average current densities at the high potential steps for each CL are

https://doi.org/10.1021/acsami.3c08377
ACS Appl. Mater. Interfaces 2023, 15, 55559−55569

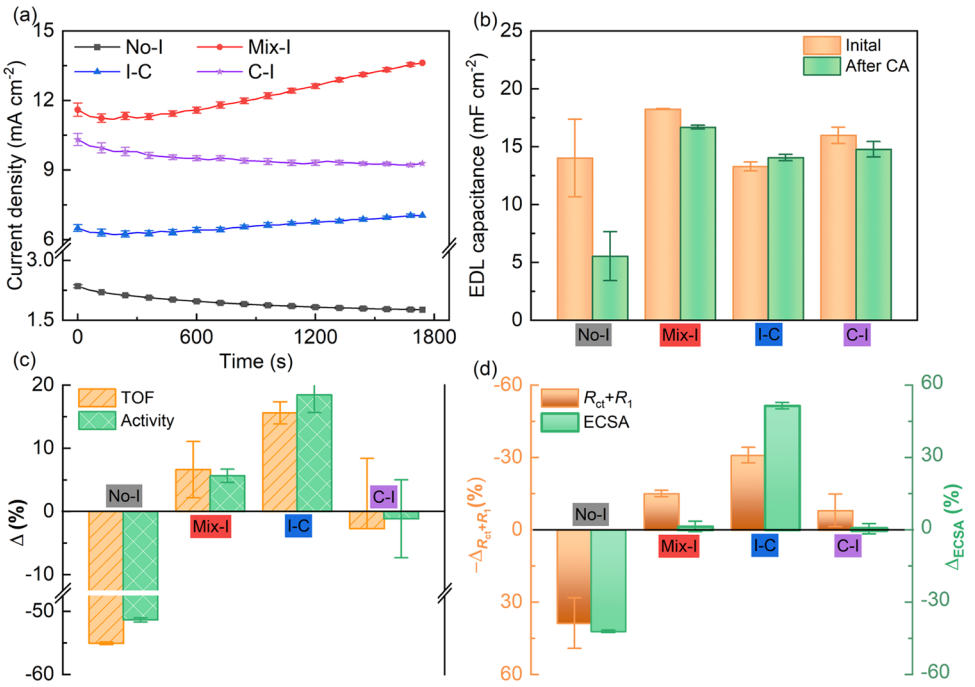

Figure 5. OER stability evaluation of IrOx by chronoamperometry (CA) measurements for different ionomer coating modes. (a) Current density at 1.55 V as a function of time, (b) EDL charging capacitance obtained by the single-point CV current method before and after CA, (c) change in TOF at *iR*-corrected voltage of 1.58 V and OER activity via LSV integrated area before and after CA, and (d) change of the total polarization resistance and ECSA before and after CA. To emphasize the performance loss, the "−" in "$\Delta R_{ct} + R_1$" is used to represent the decrease of reaction resistance.

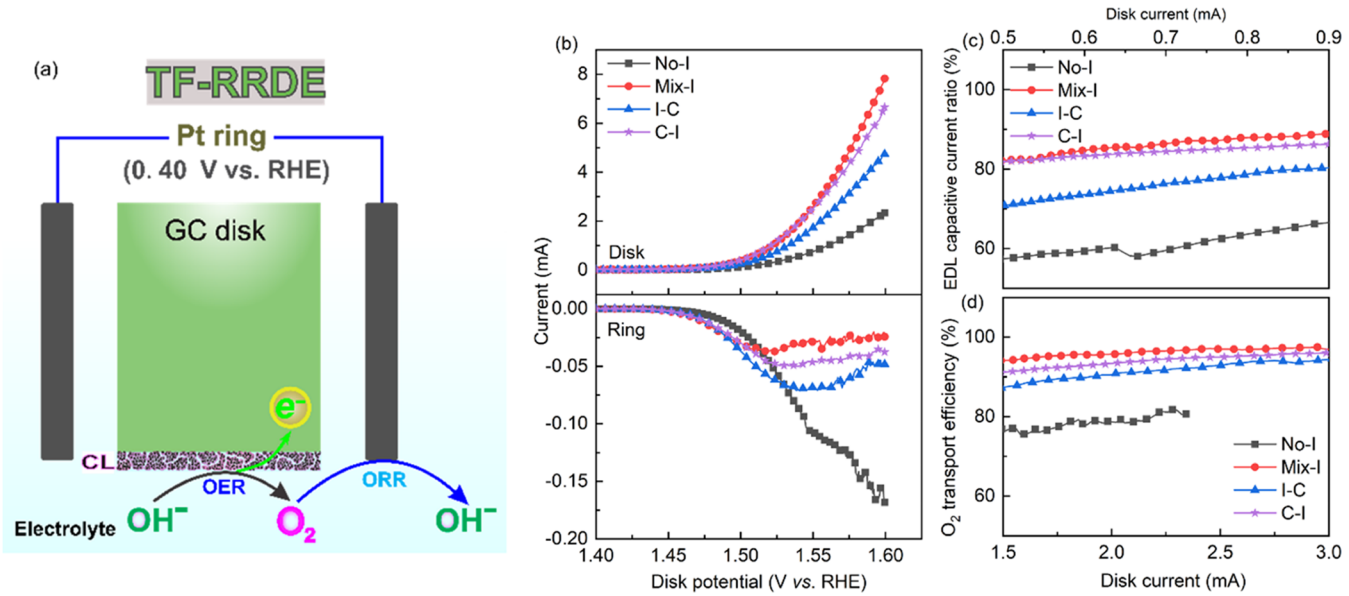

Figure 6. TF-RRDE evaluation of the effects of ionomer loading mode. (a) Schematic illustration of species transport behaviors in the TF-RRDE configuration. (b) RRDE voltammetry at the disk electrode (at a rotating rate of 2500 rpm and a scan rate of 1 mV s^{-1}) and ring electrode (held at 0.40 V vs RHE). (c) EDL capacitive current ratio and (d) O_2 transport efficiency as a function of disk current.

displayed in Figure 5a. The performance of the CLs was assessed by comparing changes in key parameters such as the TOF, the OER activity, $R_{ct} + R_1$, and the ECSA shown in Figure 5. The comparison results were calculated as follows:

$$\Delta\,(\%) = 100 \times \frac{\chi_{CA} - \chi_{initial}}{\chi_{initial}}$$

where χ_{CA} is the measured parameter after CA test and $\chi_{initial}$ is the initial measured parameter. Figure S5 presents various EDL capacitive behaviors of the CLs obtained from their CV curves. After the CA test, the EDL capacitance of the CLs was measured by using CV tests at various scan speeds (Figure S6) and compared to their initial EDL capacitance (Figure 5b). In Figure S5c, the ratio C_{outer}/C_{total} represents the apparent porosity in the CL.[56] The decrease in C_{outer}/C_{total} observed in the stability test for the CLs with Nafion can be attributed to particle agglomeration and EDL reconfiguration during the OER process. After the stability test, the C_{outer}/C_{total} increased for No-I, indicating the loss of catalyst particles without a binder in

https://doi.org/10.1021/acsami.3c08377
ACS Appl. Mater. Interfaces 2023, 15, 55559−55569

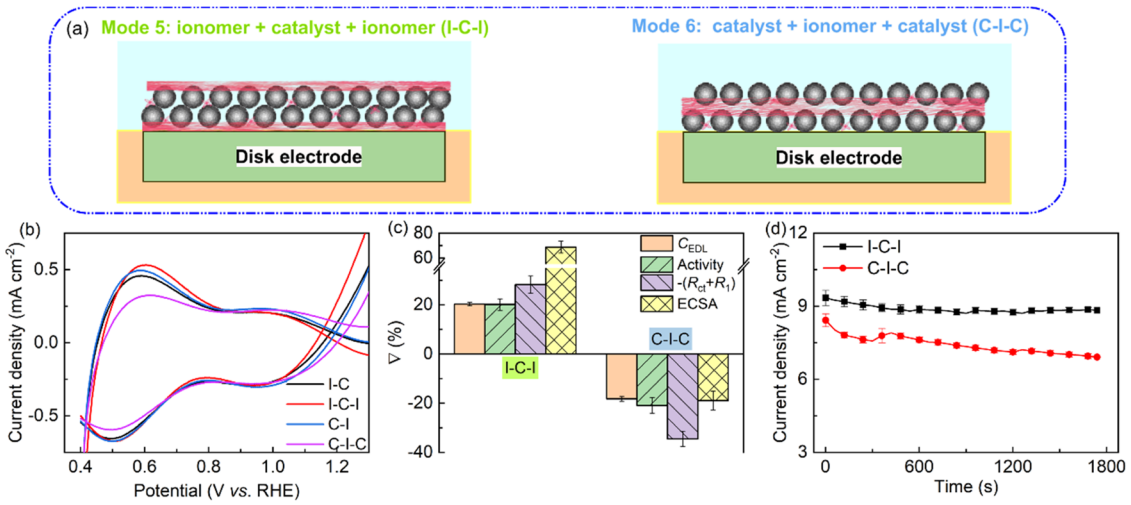

Figure 7. (a) Illustration of the coating modes I−C−I and C−I−C schematic for TF-RDE evaluation. (b) Modified CV curves at 50 mV s^{-1} to detect the pseudocapacitive behaviors. The shown current is the measured current subtracted by the EDL current at the same scan rate. (c) Performance alternation of I−C−I and C−I−C samples after the stability test when compared with I−C and C−I samples, respectively. (d) *I*−*t* curves at the high potential, 1.55 V, during CA measurement.

the CL. Figure S7 shows the SEM images of the No-I CL before and after the stability test. In Figure S7b,c, catalyst loss from the No-I CL can be clearly observed in the marked area. Figure S5d shows the interfacial reversibility, represented by the ratio of C_{EDL}^{+}/C_{EDL}^{-}, during the CV process. For CLs containing Nafion, the ratio of C_{EDL}^{+}/C_{EDL}^{-} remains around 1, showing good reversibility before and after the stability test. The C_{EDL}^{+}/C_{EDL}^{-} ratio is found to be higher than 1 for No-I before and after the stability test, confirming a lower interfacial reversibility for No-I. It is also plausible to assume that the anodic-to-cathodic capacitance ratio is connected to catalyst dissolution.[57] A higher ratio corresponds to higher anodic dissolution during the OER. The CLs without Nafion showed a greater ratio than the CLs with Nafion, indicating that Nafion is capable of successfully preventing catalyst dissolution. Figure S8 shows LSV, TOF, and Tafel plots, as well as variations in Tafel plots following the CA test. Figure 5b shows that No-I had a significant drop in EDL capacitance, while the other CLs containing Nafion ionomer had only a slight change in EDL capacitance following the CA test. Figure 5c displays the change in CL activity following the CA test as well as the corresponding change in TOF. The activity loss and TOF drop for NO-I were determined to be around 50%. For C−I, there was a small decrease in activity and TOF (around 5%). However, activity and TOF increased by around 10 and 20% for Mix-I and I−C, respectively. The change in total polarization resistance and ECSA is displayed in Figure 5d. Figure S9 shows EIS spectra at 1.55 V following a 60-step CA measurement. No-I showed a considerable increase in the overall polarization resistance and a significant decrease in the ECSA, as predicted. The CLs containing Nafion ionomer, on the other hand, showed a drop in total polarization resistance and an increase in ECSA, with I−C showing the most significant change. The changes in EDL capacitance, TOF, ECSA, and $R_{ct} + R_1$ for all CLs are consistent with their activity loss or increase. The use of Nafion as a binder in CL considerably increases catalyst particle connectivity and prevents CL detachment during stability testing. However, the addition of an excess ionomer has the potential to reduce the number of active catalytic sites, resulting in mass transfer loss. The chemical and structural reconstruction of the EDL determines how the CLs change their activity following the stability test.

The catalyst activity for the OER is determined by effective charge transfer and transport of the O_2 in the EDL. TF-RRDE voltammetry was used to quantify the contribution of various transport properties. Figure 6a illustrates a schematic of the TF-RRDE system. The disk potential was swept from 1.375 to 1.60 V at a scan rate of 2 mV s^{-1} during TF-RRDE voltammetry, and O_2 generated at the disk was detected at the ring electrode fixed at 0.4 V to reduce O_2 molecules. The faradaic mechanism might encompass an OER via a two-electron oxidation pathway, leading to the creation of an HO_2^- intermediate. To investigate this phenomenon, the ring potential was set to 1.4 V to facilitate the oxidation of HO_2^-.[24,25,58] In addition, We have also opted for a potential of 1.1 V, which is sufficiently elevated to facilitate the oxidation of H_2O_2 (in the diffusion-limited range), yet remains below the thermodynamic potential required for O_2 evolution.[43] Figure S10 reveals negligible ring current detection in both cases. This result affirms that the electrocatalytic OER facilitated by the studied IrO_2-based catalyst layers adheres to a four-electron transfer mechanism. Our previous study showed that oxygen generated during OER can be detected at the ring electrode by TF-RRDE in the low overpotential region, allowing the contribution of EDL charging to be precisely monitored.[25] Faradaic OER produces the majority of the total current generated in the high potential zone (mixed kinetic-diffusion region). Therefore, the O_2 transport efficiency can be estimated by subtracting the EDL charging current from the total disk current.

Figure 6b presents the TF-RRDE voltammetry results of various CLs. As the disk potential was scanned positively and reached the onset potential (1.4 V), the ORR current at the ring electrode began to grow, indicating the successful reduction of the O_2 generated at the disk. The ring current reached a maximum and then decreased, forming a plateau as the disk potential was scanned to a higher potential zone. This indicates mass transport limitation at the ring due to the transported O_2 from the disk. This observation suggests the presence of an O_2 bubble effect, indicating that the majority of the generated O_2 exited the disk electrode and entered the electrolyte solution

https://doi.org/10.1021/acsami.3c08377
ACS Appl. Mater. Interfaces 2023, 15, 55559−55569

without being reduced at the ring electrode.[25] The CLs with the Nafion ionomer showed a smaller ring current than No-I. In the case of No-I, the OER proceeds at a slower rate, leading to a gradual release of oxygen from the disk electrode. Therefore, oxygen can be effectively detected by the ring electrode, resulting in a higher ring current compared with the other catalyst layers with Nafion. According to our previous study, the RRDE data were further processed to obtain the EDL capacitive current ratio and oxygen transport efficiency, which are presented in Figure 6c.[25] When CLs containing Nafion were compared with those without the ionomer (No-I), the EDL capacitive current ratio was found to be substantially higher for the CLs containing Nafion. Compared to I−C, Mix-I and C−I had a comparable or greater EDL capacitive current ratio. In Figure S11, it is observed that adding the ionomer layer first and then casting the CL on top of it prevents the catalyst particles from having a proper connection and attachment to the electrode surface. In the FESEM image presented in Figure S11a, it becomes evident that the catalyst layer exhibits a loosely adhered connection with a Nafion layer that was cast before the catalyst layer itself. In Figure S11b, the catalyst layer demonstrates a reduction in particle density subsequent to the OER experiment. Furthermore, the O_2 transport efficiency of the CLs follows the same trend as their EDL capacitive current ratio, demonstrating that the Nafion ionomer in CLs functions not only as a binder but also as a transport medium capable of achieving substantial OER activity. The impact of catalyst loading on the EDL capacitive current ratio and O_2 transport efficiency has also been investigated and is shown in Figure S13. When the loading was increased to 0.24 mg cm^{-2}, the EDL capacitive current ratio and oxygen transport efficiency for the CLs with a Nafion ionomer were drastically reduced. The overlapping catalyst surface rendered the catalytic active sites inaccessible to the reactants. The lower porosity of the CLs due to the higher loading caused a decrease in the O_2 transport efficiency. It is worth highlighting that the magnitude of the EDL capacitive current ratio and the O_2 transport efficiency of the catalyst layers will reduce if we consider a lower collection efficiency than the geometric collection efficiency (37.3%). However, the overall trend remains consistent and the comparisons among the four Nafion ionomer deposition modes are still valid.

We investigated the influence of CL configuration on electrochemical parameters using a three-layer structure, namely, I−C−I and C−I−C, as schematically illustrated in Figure 7a,b. In Figure 7c, we assessed the role Nafion ionomer in building an efficient mass transport network by calculating the alternation percentage, ∇(%), between key parameters, ψ, obtained from TF-RDE tests, including C_{EDL}, OER activity, $-(R_{ct} + R_1)$, and ECSA. The calculation is as follows:

$$\nabla(\%) = 100 \times \frac{\psi_{new} - \psi_s}{\psi_s}$$

where ψ_{new} and ψ_s refer to the properties obtained from the new sample and the corresponding reference sample, respectively. The reference sample is either I−C (for the new sample, I−C−I) or C−I (for C−I−C). Raw experimental data of I−C−I and C−I−C are presented in Figures S14−S16, which were used to calculate the change in essential parameters illustrated in Figure 7c,7d. When comparing I−C−I and C−I−C to I−C and C−I, respectively, we observed that the overpotential at 10 mA cm^{-2} remains the same, as indicated by the LSV curves in Figure S14c. Apart from a significant positive change in C_{EDL} following the stability test, the major electrochemical parameters for I−C−I remain unaltered. Moreover, compared with I−C, the current densities during the stability test are higher. These findings suggest that adding Nafion to the top of the CL I−C not only serves as a binder to minimize catalyst loss but also enhances catalyst connection and accessibility to active catalyst sites. On the other hand, adding CL to the top of the ionomer layer in C−I makes the catalyst particles more prone to detachment during the OER test and reduces catalyst particle connection. As a result, during the stability test, C−I−C exhibited a negative shift in key electrochemical parameters and lower current densities. Although adjusting the drop-casting process can potentially improve the activity and stability of CLs, our results show that a catalyst ink containing well-dispersed Nafion ionomer produces the best CL with superior activity and stability for OER. This can be attributed to the homogeneous distribution of the ionomer in the CL. Furthermore, following the stability test, the OER activity of I−C increased more than that of Mix-I. This can be attributed to the cyclic transition of hydroxylated metal cations with various oxidation states, leading to reconstruction.[17,59] Continuous EDL reconstruction appears to be advantageous for OH^- adsorption in Mix-I and I−C. Hence, achieving an optimal distribution of Nafion in the CL is crucial to ensure the required adhesion to GCE, efficient charge transport, and prevention of catalyst dissolution during the OER, resulting in increased activity and stability of the IrOx catalyst material.

4. CONCLUSIONS

In conclusion, this study investigated the role of Nafion in different modes of catalyst loading for the OER in an alkaline medium. The CLs containing Nafion ionomer exhibited significantly lower overpotential in the kinetic region (10 mA cm^{-2}) compared to Nafion-free CLs (No-I). The turnover frequency of Mix-I was approximately twice as high as that of No-I. This indicates that the presence of Nafion not only improves CL adhesion but also enhances catalyst particle connection and intrinsic OER activity. However, a higher loading was found to negatively affect the EDL charging capacitance and the O_2 transport efficiency of the CLs. By adding Nafion to catalyst inks, interfacial reversibility is improved, and anodic dissolution of IrO_x is prevented, as supported by the investigation of EDL capacitive behavior. Additionally, achieving the proper distribution of Nafion ionomer in the CL can further enhance OER catalytic activity. The findings of this study underscore the indispensable role of Nafion ionomer and its crucial interaction with the catalyst through various processing modes for OER. These combined results offer fresh insights into the optimal electrode design for electrolysis cells in hydrogen technology.

■ ASSOCIATED CONTENT

Supporting Information

The Supporting Information is available free of charge at https://pubs.acs.org/doi/10.1021/acsami.3c08377.

Additional information on tables of impedance fitting parameters, FESEM images of the catalyst layers, and figures of electrochemical results (PDF)

https://doi.org/10.1021/acsami.3c08377
ACS Appl. Mater. Interfaces 2023, 15, 55559−55569

AUTHOR INFORMATION

Corresponding Authors

Guangfu Li − *Department of Mechanical Engineering, University of California, Merced, Merced, California 95343, United States; Foshan Xianhu Laboratory of the Advanced Energy Science and Technology, Guangdong Laboratory, Foshan 528200, China*; Email: liguangfu@xhlab.cn

Po-Ya Abel Chuang − *Department of Mechanical Engineering, University of California, Merced, Merced, California 95343, United States;* orcid.org/0000-0002-0440-1974; Email: abel.chuang@ucmerced.edu

Authors

Nitul Kakati − *Department of Mechanical Engineering, University of California, Merced, Merced, California 95343, United States*

Lawrence Anderson − *Department of Mechanical Engineering, University of California, Merced, Merced, California 95343, United States*

Desiree Mae Sua-an − *Department of Mechanical Engineering, University of California, Merced, Merced, California 95343, United States; Laboratory of Electrochemical Engineering, Department of Chemical Engineering, University of the Philippines Diliman, Quezon City 1101, Philippines*

Ayon Karmakar − *Department of Mechanical Engineering, University of California, Merced, Merced, California 95343, United States;* orcid.org/0000-0002-9854-5185

Joey D. Ocon − *Laboratory of Electrochemical Engineering, Department of Chemical Engineering, University of the Philippines Diliman, Quezon City 1101, Philippines*

Complete contact information is available at: https://pubs.acs.org/10.1021/acsami.3c08377

Author Contributions

The manuscript was written through contributions of all authors. All authors have given approval to the final version of the manuscript.

Notes

The authors declare no competing financial interest.

ACKNOWLEDGMENTS

This work was supported by the University of California, Merced and the CIPHER Program (IIID 2018-008) from the Commission on Higher Education-Philippine California Advanced Research Institutes (CHED-PCARI) of the Republic of the Philippines. FESEM experiments were performed at Imaging and Microscopy Facility (IMF) at UC Merced. The authors also thank all of their laboratory members, especially Mrittunjoy Sarker, for the insightful discussions and support.

REFERENCES

(1) Sazali, N. Emerging Technologies by Hydrogen: A Review. *Int. J. Hydrogen Energy* **2020**, *45* (38), 18753−18771.

(2) Boretti, A. Production of Hydrogen for Export from Wind and Solar Energy, Natural Gas, and Coal in Australia. *Int. J. Hydrogen Energy* **2020**, *45* (7), 3899−3904.

(3) Hales, N.; Schmidt, T. J.; Fabbri, E. Reversible and Irreversible Transformations of Ni-Based Electrocatalysts during the Oxygen Evolution Reaction. *Curr. Opin. Electrochem.* **2023**, *38*, No. 101231.

(4) Anantharaj, S.; Kundu, S.; Noda, S. The Fe Effect": A Review Unveiling the Critical Roles of Fe in Enhancing OER Activity of Ni and Co Based Catalysts. *Nano Energy* **2021**, *80*, No. 105514.

(5) Park, D. H.; Kim, M. H.; Kim, M.; Byeon, J. H.; Jang, J. S.; Kim, J. H.; Lim, D. M.; Park, S. H.; Gu, Y. H.; Kim, J.; Park, K. W. Spherical Nickel Doped Cobalt Phosphide as an Anode Catalyst for Oxygen Evolution Reaction in Alkaline Media: From Catalysis to System. *Appl. Catal., B* **2023**, *327*, No. 122444.

(6) Mefford, J. T.; Rong, X.; Abakumov, A. M.; Hardin, W. G.; Dai, S.; Kolpak, A. M.; Johnston, K. P.; Stevenson, K. J. Water Electrolysis on La1-XSrxCoO3-δ Perovskite Electrocatalysts. *Nat. Commun.* **2016**, *7*, No. 11053, DOI: 10.1038/ncomms11053.

(7) Tian, Z. Y.; Han, X. Q.; Du, J.; Li, Z. B.; Ma, Y. Y.; Han, Z. G. Bio-Inspired FeMo2S4Microspheres as Bifunctional Electrocatalysts for Boosting Hydrogen Oxidation/Evolution Reactions in Alkaline Solution. *ACS Appl. Mater. Interfaces* **2023**, *15* (9), 11853−11865.

(8) Selvasundarasekar, S. S.; Bijoy, T. K.; Kumaravel, S.; Karmakar, A.; Madhu, R.; Bera, K.; Nagappan, S.; Dhandapani, H. N.; Mersal, G. A. M.; Ibrahim, M. M.; Sarkar, D.; Yusuf, S. M.; Lee, S. C.; Kundu, S. Effective Formation of a Mn-ZIF-67 Nanofibrous Network via Electrospinning: An Active Electrocatalyst for OER in Alkaline Medium. *ACS Appl. Mater. Interfaces* **2022**, *14* (41), 46581−46594.

(9) Burke, M. S.; Enman, L. J.; Batchellor, A. S.; Zou, S.; Boettcher, S. W. Oxygen Evolution Reaction Electrocatalysis on Transition Metal Oxides and (Oxy)Hydroxides: Activity Trends and Design Principles. *Chem. Mater.* **2015**, *27* (22), 7549−7558.

(10) Varcoe, J. R.; Atanassov, P.; Dekel, D. R.; Herring, A. M.; Hickner, M. A.; Kohl, P. A.; Kucernak, A. R.; Mustain, W. E.; Nijmeijer, K.; Scott, K.; Xu, T.; Zhuang, L. Anion-Exchange Membranes in Electrochemical Energy Systems. *Energy Environ. Sci.* **2014**, *7* (10), 3135−3191.

(11) Li, X.; Hao, X.; Abudula, A.; Guan, G. Nanostructured Catalysts for Electrochemical Water Splitting: Current State and Prospects. *J. Mater. Chem. A* **2016**, *4* (31), 11973−12000.

(12) Swesi, A. T.; Masud, J.; Nath, M. Nickel Selenide as a High-Efficiency Catalyst for Oxygen Evolution Reaction. *Energy Environ. Sci.* **2016**, *9* (5), 1771−1782.

(13) Pavel, C. C.; Cecconi, F.; Emiliani, C.; Santiccioli, S.; Scaffidi, A.; Catanorchi, S.; Comotti, M. Highly Efficient Platinum Group Metal Free Based Membrane-Electrode Assembly for Anion Exchange Membrane Water Electrolysis. *Angew. Chem.* **2014**, *126* (5), 1402−1405.

(14) Thangavel, P.; Ha, M.; Kumaraguru, S.; Meena, A.; Singh, A. N.; Harzandi, A. M.; Kim, K. S. Graphene-Nanoplatelets-Supported NiFe-MOF: High-Efficiency and Ultra-Stable Oxygen Electrodes for Sustained Alkaline Anion Exchange Membrane Water Electrolysis. *Energy Environ. Sci.* **2020**, *13*, 3447.

(15) Danilovic, N.; Subbaraman, R.; Chang, K.; Chang, S. H.; Kang, Y. J.; Snyder, J.; Paulikas, A. P.; Strmcnik, D.; Kim, Y.; Myers, D.; Stamenkovic, V. R.; Markovic, N. M. Activity − Stability Trends for the Oxygen Evolution Reaction on Monometallic Oxides in Acidic Environments. *J. Phys. Chem. Lett.* **2014**, *5*, 2474−2478, DOI: 10.1021/jz501061n.

(16) Yu, Z. Y.; Lang, C. C.; Gao, M. R.; Chen, Y.; Fu, Q. Q.; Duan, Y.; Yu, S. H. Ni-Mo-O Nanorod-Derived Composite Catalysts for Efficient Alkaline Water-to-Hydrogen Conversion: Via Urea Electrolysis. *Energy Environ. Sci.* **2018**, *11* (7), 1890−1897.

(17) Spöri, C.; Kwan, J. T. H.; Bonakdarpour, A.; et al. The Stability Challenges of Oxygen Evolving Catalysts: Towards a Common Fundamental Understanding and Mitigation of Catalyst Degradation. *Angew. Chem., Int. Ed.* **2016**, *56*, 5994−6021, DOI: 10.1002/anie.201608601.

(18) Suen, N. T.; Hung, S. F.; Quan, Q.; Zhang, N.; Xu, Y. J.; Chen, H. M. Electrocatalysis for the Oxygen Evolution Reaction: Recent Development and Future Perspectives. *Chem. Soc. Rev.* **2017**, *46* (2), 337−365.

(19) Ganassin, A.; Maljusch, A.; Colic, V.; Spanier, L.; Brandl, K.; Schuhmann, W.; Bandarenka, A. Benchmarking the Performance of Thin-Film Oxide Electrocatalysts for Gas Evolution Reactions at High Current Densities. *ACS Catal.* **2016**, *6* (5), 3017−3024.

(20) McCrory, C. C. L.; Jung, S.; Peters, J. C.; Jaramillo, T. F. Benchmarking Heterogeneous Electrocatalysts for the Oxygen Evolution Reaction. *J. Am. Chem. Soc.* **2013**, *135* (45), 16977−16987.
(21) McCrory, C. C. L.; Jung, S.; Ferrer, I. M.; Chatman, S. M.; Peters, J. C.; Jaramillo, T. F. Benchmarking Hydrogen Evolving Reaction and Oxygen Evolving Reaction Electrocatalysts for Solar Water Splitting Devices. *J. Am. Chem. Soc.* **2015**, *137* (13), 4347−4357.
(22) Grimaud, A.; Demortiere, A.; Saubanere, M.; Dachraoui, W.; Duchamp, M.; Doublet, M. L.; Tarascon, J. M. Activation of Surface Oxygen Sites on an Iridium-Based Model Catalyst for the Oxygen Evolution Reaction. *Nat. Energy* **2017**, *2* (1), No. 16189, DOI: 10.1038/nenergy.2016.189.
(23) Li, G. F.; Divinagracia, M.; Labata, M. F.; Ocon, J. D.; Abel Chuang, P. Y. Electrolyte-Dependent Oxygen Evolution Reactions in Alkaline Media: Electrical Double Layer and Interfacial Interactions. *ACS Appl. Mater. Interfaces* **2019**, *11* (37), 33748−33758.
(24) Li, G. F.; Yang, D.; Abel Chuang, P. Y. Defining Nafion Ionomer Roles for Enhancing Alkaline Oxygen Evolution Electrocatalysis. *ACS Catal.* **2018**, *8* (12), 11688−11698.
(25) Li, G.; Anderson, L.; Chen, Y.; Pan, M.; Abel Chuang, P. Y. New Insights into Evaluating Catalyst Activity and Stability for Oxygen Evolution Reactions in Alkaline Media. *Sustainable Energy Fuels* **2018**, *2* (1), 237−251.
(26) Li, G.; Chuang, P. Y. A. Identifying the Forefront of Electrocatalytic Oxygen Evolution Reaction: Electronic Double Layer. *Appl. Catal., B* **2018**, *239*, 425−432.
(27) Kakati, N.; Li, G.; Chuang, P. Y. A. Insights into the Ni/C-Based Thin-Film Catalyst Layer Design for Urea Oxidation Reaction in a Three-Electrode System. *ACS Appl. Energy Mater.* **2021**, *4* (4), 4224−4233.
(28) del Rosario, J. A. D.; Li, G.; Labata, M. F. M.; Ocon, J. D.; Chuang, P. Y. A. Unravelling the Roles of Alkali-Metal Cations for the Enhanced Oxygen Evolution Reaction in Alkaline Media. *Appl. Catal., B* **2021**, *288*, No. 119981.
(29) Labata, M. F.; Li, G.; Ocon, J.; Chuang, P. Y. A. Insights on Platinum-Carbon Catalyst Degradation Mechanism for Oxygen Reduction Reaction in Acidic and Alkaline Media. *J. Power Sources* **2021**, *487*, No. 229356.
(30) Riasse, R.; Lafforgue, C.; Vandenberghe, F.; Micoud, F.; Morin, A.; Arenz, M.; Durst, J.; Chatenet, M. Benchmarking Proton Exchange Membrane Fuel Cell Cathode Catalyst at High Current Density: A Comparison between the Rotating Disk Electrode, the Gas Diffusion Electrode and Differential Cell. *J. Power Sources* **2023**, *556*, No. 232491, DOI: 10.1016/j.jpowsour.2022.232491.
(31) Ke, K.; Hiroshima, K.; Kamitaka, Y.; Hatanaka, T.; Morimoto, Y. An Accurate Evaluation for the Activity of Nano-Sized Electrocatalysts by a Thin-Film Rotating Disk Electrode: Oxygen Reduction on Pt/C. *Electrochim. Acta* **2012**, *72*, 120−128.
(32) Nesselberger, M.; Ashton, S.; Meier, J. C.; Katsounaros, I.; Mayrhofer, K. J. J.; Arenz, M. The Particle Size Effect on the Oxygen Reduction Reaction Activity of Pt Catalysts: Influence of Electrolyte and Relation to Single Crystal Models. *J. Am. Chem. Soc.* **2011**, *133* (43), 17428−17433.
(33) Takahashi, I.; Kocha, S. S. Examination of the Activity and Durability of PEMFC Catalysts in Liquid Electrolytes. *J. Power Sources* **2010**, *195* (19), 6312−6322.
(34) Li, K.; Yu, S.; Li, D.; Ding, L.; Wang, W.; Xie, Z.; Park, E. J.; Fujimoto, C.; Cullen, D. A.; Kim, Y. S.; Zhang, F. Y. Engineered Thin Diffusion Layers for Anion-Exchange Membrane Electrolyzer Cells with Outstanding Performance. *ACS Appl. Mater. Interfaces* **2021**, *13* (43), 50957−50964.
(35) Garsany, Y.; Singer, I. L.; Swider-Lyons, K. E. Impact of Film Drying Procedures on RDE Characterization of Pt/VC Electrocatalysts. *J. Electroanal. Chem.* **2011**, *662* (2), 396−406.
(36) Garsany, Y.; Baturina, O. A.; Swider-Lyons, K. E.; Kocha, S. S. Experimental Methods for Quantifying the Activity of Platinum Electrocatalysts for the Oxygen Reduction Reaction. *Anal. Chem.* **2010**, *82* (15), 6321−6328.
(37) Yang, D.; Guo, Y.; Tang, H.; Wang, Y.; Yang, D.; Ming, P.; Zhang, C.; Li, B.; Zhu, S. Influence of the Dispersion State of Ionomer on the Dispersion of Catalyst Ink and the Construction of Catalyst Layer. *Int. J. Hydrogen Energy* **2021**, *46* (66), 33300−33313.
(38) Rodríguez, L. G.; Campana Prada, R.; Sanchez-Molina, M.; Rodríguez Victoria, T. A. Study of the Influence of Nafion/C Composition on Electrochemical Performance of PEM Single Cells with Ultra-Low Platinum Load. *Int. J. Hydrogen Energy* **2020**, *6*, 17550−17561.
(39) Ott, S.; Orfanidi, A.; Schmies, H.; Anke, B.; Nong, H. N.; Hübner, J.; Gernert, U.; Gliech, M.; Lerch, M.; Strasser, P. Ionomer Distribution Control in Porous Carbon-Supported Catalyst Layers for High-Power and Low Pt-Loaded Proton Exchange Membrane Fuel Cells. *Nat. Mater.* **2020**, *19* (1), 77−85.
(40) Zhang, J.; Zhu, W.; Huang, T.; Zheng, C.; Pei, Y.; Shen, G.; Nie, Z.; Xiao, D.; Yin, Y.; Guiver, M. D. Recent Insights on Catalyst Layers for Anion Exchange Membrane Fuel Cells. *Adv. Sci.* **2021**, *8*, No. 2100284.
(41) Lopez-Haro, M.; Guétaz, L.; Printemps, T.; Morin, A.; Escribano, S.; Jouneau, P. H.; Bayle-Guillemaud, P.; Chandezon, F.; Gebel, G. Three-Dimensional Analysis of Nafion Layers in Fuel Cell Electrodes. *Nat. Commun.* **2014**, *5*, No. 5229.
(42) Lu, W.; Shao, Z. G.; Zhang, G.; Zhao, Y.; Li, J.; Yi, B. Preparation and Characterization of Imidazolium-Functionalized Poly (Ether Sulfone) as Anion Exchange Membrane and Ionomer for Fuel Cell Application. *Int. J. Hydrogen Energy* **2013**, *38* (22), 9285−9296.
(43) Chung, D. Y.; Lopes, P. P.; Farinazzo Bergamo Dias Martins, P.; He, H.; Kawaguchi, T.; Zapol, P.; You, H.; Tripkovic, D.; Strmcnik, D.; Zhu, Y.; Seifert, S.; Lee, S.; Stamenkovic, V. R.; Markovic, N. M. Dynamic Stability of Active Sites in Hydr(Oxy)Oxides for the Oxygen Evolution Reaction. *Nat. Energy* **2020**, *5* (3), 222−230.
(44) Bladergroen, B.; Su, H.et al. *Overview of Membrane Electrode Assembly Preparation Methods for Solid Polymer Electrolyte Electrolyzer*; IntechOpen, 2023.
(45) Bae, J. H.; Han, J.; Chung, T. D.*Electrochemistry at Nanoporous Interfaces : New Opportunity for Electrocatalysis*; InTech, 2012; pp 448−463.
(46) Bard, A. J.; Faulkner, L. R. *Electrochemical Methods, Fundamentals and Applications*, 2nd ed.; John Wiley & Sons, Inc., 2001.
(47) Costentin, C.; Porter, T. R.; Savéant, J. M. Conduction and Reactivity in Heterogeneous-Molecular Catalysis: New Insights in Water Oxidation Catalysis by Phosphate Cobalt Oxide Films. *J. Am. Chem. Soc.* **2016**, *138* (17), 5615−5622.
(48) Giménez, S.; Bisquert, J. *Photoelectrochemical Solar Fuel Production: From Basic Principles to Advanced Devices*; Springer, 2016.
(49) El-Sayed, H. A.; Weiß, A.; Olbrich, L. F.; Putro, G. P.; Gasteiger, H. A. OER Catalyst Stability Investigation Using RDE Technique: A Stability Measure or an Artifact? *J. Electrochem. Soc.* **2019**, *166* (8), F458−F464.
(50) Lazaridis, T.; Stühmeier, B. M.; Gasteiger, H. A.; El-Sayed, H. A. Capabilities and Limitations of Rotating Disk Electrodes versus Membrane Electrode Assemblies in the Investigation of Electrocatalysts. *Nat. Catal.* **2022**, *5* (5), 363−373.
(51) Bae, J. H.; Han, J. H.; Chung, T. D. Electrochemistry at Nanoporous Interfaces: New Opportunity for Electrocatalysis. *Phys. Chem. Chem. Phys.* **2012**, *14* (2), 448−463.
(52) Li, H.; Chen, Z.; Yu, Q.; Zhu, W.; Cui, W. Effects of Tungsten Carbide on the Electrocatalytic Activity of PbO 2 -WC Composite Inert Anodes during Zinc Electrowinning. *J. Electrochem. Soc.* **2017**, *164* (14), H1064−H1071.
(53) He, C.; Tao, J. Three-Dimensional Hollow Porous Co6Mo6C Nanoframe as an Highly Active and Durable Electrocatalyst for Water Splitting. *J. Catal.* **2017**, *347*, 63−71.
(54) Cho, M. K.; Park, H. Y.; Lee, H. J.; Kim, H. J.; Lim, A.; Henkensmeier, D.; Yoo, S. J.; Kim, J. Y.; Lee, S. Y.; Park, H. S.; Jang, J. H. Alkaline Anion Exchange Membrane Water Electrolysis: Effects of Electrolyte Feed Method and Electrode Binder Content. *J. Power Sources* **2018**, *382*, 22−29.

(55) Hiesgen, R.; Morawietz, T.; Handl, M.; Corasaniti, M.; Friedrich, K. A. Insight into the Structure and Nanoscale Conductivity of Fluorinated Ionomer Membranes. *J. Electrochem. Soc.* **2014**, *161* (12), F1214−F1223.
(56) Li, G.; Yu, H.; Song, W.; Wang, X.; Li, Y.; Shao, Z.; Yi, B. Zeolite-Templated Ir XRu 1-XO 2 Electrocatalysts for Oxygen Evolution Reaction in Solid Polymer Electrolyte Water Electrolyzers. *Int. J. Hydrogen Energy* **2012**, *37* (22), 16786−16794.
(57) Rand, D. A. J.; Woods, R. A Study of the Dissolution of Platinum, Palladium, Rhodium and Gold Electrodes in 1 m Sulphuric Acid by Cyclic Voltammetry. *J. Electroanal. Chem. Interfacial Electrochem.* **1972**, *35* (1), 209−218.
(58) Davodi, F.; Tavakkoli, M.; Lahtinen, J.; Kallio, T. Straightforward Synthesis of Nitrogen-Doped Carbon Nanotubes as Highly Active Bifunctional Electrocatalysts for Full Water Splitting. *J. Catal.* **2017**, *353*, 19−27.
(59) Brodsky, C. N.; Hadt, R. G.; Hayes, D.; Reinhart, B. J.; Li, N.; Chen, L. X.; Nocera, D. G. In Situ Characterization of Cofacial Co(IV) Centers in Co4O4 Cubane: Modeling the High-Valent Active Site in Oxygen-Evolving Catalysts. *Proc. Natl. Acad. Sci. U.S.A.* **2017**, *114* (15), 3855−3860.

https://doi.org/10.1021/acsami.3c08377
ACS Appl. Mater. Interfaces 2023, 15, 55559−55569